JAAS

PAPER

View Article Online
View Journal | View Issue

Cite this: *J. Anal. At. Spectrom.*, 2018, 33, 613

Multi-element ion-exchange chromatography and high-precision MC-ICP-MS isotope analysis of Mg and Ti from sub-mm-sized meteorite inclusions†

K. K. Larsen, * D. Wielandt and M. Bizzarro

The analytical improvement of new generation mass spectrometers has reached a level required for high-precision isotope analysis of very small and unique natural samples. The multi-element isotopic signatures of meteorite inclusions can potentially provide detailed insight into the origin of our solar system. As such, in-line separation and isotope analysis of multiple elements from such unique samples is highly desirable, but rarely accommodated by current chromatographic purification procedures necessary for accurate isotope analysis using multiple collector inductively coupled plasma source mass spectrometry (MC-ICP-MS). Here, we report a new multi-element ion chromatographic purification procedure, specifically developed for the separation of very small amounts of Mg (~5 μg) and Ti (0.7–1 μg) from individual samples. Highly isotopically anomalous sub-mm sized materials, such as Ca–Al-rich inclusions in primitive meteorites, can be routinely analysed for their mass-independent μ^{26}Mg*, μ^{46}Ti*, μ^{48}Ti*, μ^{49}Ti* and μ^{50}Ti* isotope compositions with an estimated external reproducibility of 4.1, 11, 8.8, 18 and 12 ppm (2sd), respectively. These procedures consume significantly less material than previous methods and as such represents a 6- to 10-fold improvement in precision. The method ensures >99.9% Mg and >97% Ti recovery, thereby allowing for the accurate determination of mass-dependent compositions with a precision better than ~60 ppm amu^{-1} for both Mg and Ti. It can further be adapted to accommodate the in-line separation of *e.g.* Ca, Cr, Fe, Ni, W, Mo, Ru, V, Zr and Hf from the same sample matrices. Doping tests on a synthetic Ti standard demonstrate that isobaric interference can be adequately corrected for provided that atomic ratios are Ca/Ti < 0.07, V/Ti < 0.04 and Cr/Ti < 0.005 and Zr^{2+}, Mo^{2+} and Ru^{2+} have no influence on Ti measurements when atomic ratios are Zr/Ti < 0.002, Mo/Ti < 0.01 and Ru/Ti < 0.001, which is ensured by the chromatographic procedures. Magnesium and titanium isotope data for terrestrial geostandards and isotopically anomalous chondrite meteorites (OC, CR, CV, and CI) and two CV CAIs are in excellent agreement with literature values, demonstrating the accuracy of our methods. The two CAIs plot on an extension of the mass-independent correlation line between μ^{46}Ti* and μ^{50}Ti* defined by inner solar system materials, suggesting residual nucleosynthetic effects in CAI precursors.

Received 27th November 2017
Accepted 10th January 2018

DOI: 10.1039/c7ja00392g

rsc.li/jaas

1. Introduction

Magnesium and titanium are both important elements in natural environments on Earth and throughout the solar system. While Mg is an important ingredient of terrestrial planets,[1] Ti is a major refractory element, which are enriched in the solar system's first solids, Ca–Al-rich inclusions (CAIs), found in primitive meteorites.[2] Studying their isotope composition potentially provides constraints on, for example, the timing and efficiency of planetary differentiation processes,[3–6] mixing and transport of primitive components in the solar protoplanetary disk,[7–9] thermal processing of presolar dust,[10] nucleosynthetic sources that contributed to the astrophysical birth environment of our young Sun,[11] biogeochemical processes on Earth[12] and evaporation and condensation processes.[13,14]

Given that Mg is a moderately volatile element and Ti a highly refractory one, potential differences in the degree of stable isotope fractionation may discern the condensation and/or evaporation history of CAIs. Also, the identification of planetary-scale mass-independent heterogeneity in both Mg (most likely associated with heterogeneities in the short-lived radioactive nuclide ^{26}Al[15–17]) and Ti isotopes[10] calls for an evaluation of the large-scale mixing/unmixing processes of pre-solar components associated with the establishment of the protoplanetary disk and the formation of the first planetesimals. The coupled isotope systematics of various elements

Centre for Star and Planet Formation, Natural History Museum of Denmark, University of Copenhagen, DK-1350, Denmark. E-mail: kirstenl@snm.ku.dk

† Electronic supplementary information (ESI) available. See DOI: 10.1039/c7ja00392g

(including Mg and Ti) from unique solar system components, including disk solids such as CAIs, AOAs (Amoeboid Olivine Aggregates) and chondrules from primitive meteorites, may aid in such a quest.

Ion chromatographic purification required for high-precision isotope analysis using Multi-Collector Inductively Coupled Plasma Mass Spectrometry (MC-ICP-MS) and Thermal Ionisation Mass Spectrometry (TIMS) is often accomplished using chromatographic separation protocols tailored for specific elements involving a combination of various ion exchangers.[18–20] The combined analysis of the isotope composition of multiple elements extracted from the exact same sample matrices may, however, be very valuable for a critical evaluation of their prehistory. Such multi-element isotope analyses are especially advantageous when handling small and unique samples, such as sub-mm meteoritic inclusions.

With the advent of new generation high-precision mass spectrometers, such as the Thermo Scientific Neptune Plus MC-ICP-MS and its Jet/X cone interface, the precision of isotope measurements has increased significantly. This has unlocked the possibility of precisely analysing very small amounts of analytes for the isotope composition of sub-mm inclusions in primitive meteorites. However, such an increase in analytical precision further tightens the demands on ion chromatographic purification protocols required to diminish the number of matrix elements generating instrumental interference and thus inaccurate measurements. It also puts constraints on the amount of impurities, known as 'blanks', introduced through chemical purification of the analyte. The scarcity of material available in small silicate samples calls for effective purification procedures that allow for the separation and high-precision isotope analysis of many elements from the same samples, while at the same time minimizing impurities introduced into the sample through chemical processing.

Given these requirements, we present a novel multi-element chromatographic separation protocol that allows for high-precision isotope analysis of Mg and Ti from the same digestion aliquots of small silicate samples. We show that sub-mm meteoritic inclusions, such as highly isotopically anomalous CAIs, can be accurately and precisely measured for their Mg and Ti isotope compositions with a resolution significantly exceeding that required to resolve mass-dependent and mass-independent variability amongst most inner solar system materials.

2. Sample preparation and ion exchange chromatography

2.1 Materials, reagents and sample digestion

Experimental and analytical procedures were carried out in ultra-clean laboratory environments with HEPA-filtered laminar flow hoods. All reagents were either purchased as ultrapure chemicals (HF, H_2O_2, and NH_4OH) or purified through distillation (HNO_3, HCl, acetone, and Milli-Q water). These reagents were all blank tested to ensure a sufficiently low level of impurities prior to chromatographic purification. CAIs were microdrilled using tungsten-carbide drill bits on a computer-assisted New Wave Micromill at the Centre for Star and Planet Formation, University of Copenhagen. Whole-rock powders, crushed silicate rock specimens and microdrilled samples (0.1–2 mg) were digested in Savillex PFA beakers in a mixture of concentrated HF : HNO_3 (3 : 1) (~0.5 ml) for 2 days at 120 °C and evaporated to dryness. To ensure complete dissolution of all samples, this step was followed by digestion in concentrated aqua regia (HCl : HNO_3 = 3 : 1) (~0.5 ml) at 120 °C for another 2 days, thereby also destroying any fluorides formed during HF–HNO_3 digestion. The aqua regia treatment was repeated until there were no remaining solids. Prior to sample digestion all PFA beakers were pre-cleaned using the same mixture of acids as that used for sample digestion. Following decomposition, all samples were converted to NO_3 salts through two evaporation cycles with 7 M HNO_3 in preparation for chromatographic purification.

2.2 In-line chromatographic separation and purification of Mg and Ti

To ensure a minimum impurity contribution from resin and reagents, we developed a new low-level chromatographic separation protocol for in-line separation and purification of multiple elements from small amounts of silicate samples. This ensures a sample load of <5% of the full cation exchange capacity (CEC) of the 1st chromatographic column, thereby preventing peak fronting during elution and thus ensuring the availability of sufficient ion exchange sites.[21] For the current setup of the exchanger columns, this corresponds to a typical sample load of approximately 1–2 mg (from which Si has been removed prior to chromatographic separation by volatilization through HF–HNO_3 digestion) depending on cation valences in individual sample matrices. The capacity of the exchanger columns can be scaled up to accommodate larger amounts of samples. This may be of relevance for the separation of elements, such as W, Mo, Ru, V, Zr and Hf, given their common presence in trace amounts in most types of sample matrices.

The ion chromatographic separation protocol involves a series of discrete ion chromatographic separation steps, as summarized in Fig. 1. It takes advantage of novel sample pre-treatment procedures to ensure a high Cr recovery (>95%)[22] and is further refined from a Mg purification protocol for larger samples (~100 μg Mg), known to provide high-purity Mg for high-precision isotope analysis by MC-ICP-MS.[23] Although applicable to most types of inorganic sample matrices, the purification method described here is specifically tailored for samples with highly anomalous isotope compositions whose measured isotope composition may be compromised by minute analyte impurity contributions. The protocol is well suited for sample matrices with particularly high amounts of Mg, Al, Ca and Fe, such as CAIs and chondrules.

Sample pre-treatment procedures for Cr speciation prior to using the 1st column. The extremely sluggish kinetics of Cr speciation in acidic media at room temperature and the large differences in the selectivity of a cation exchanger for various Cr(III) species are known to be problematic for high Cr recovery

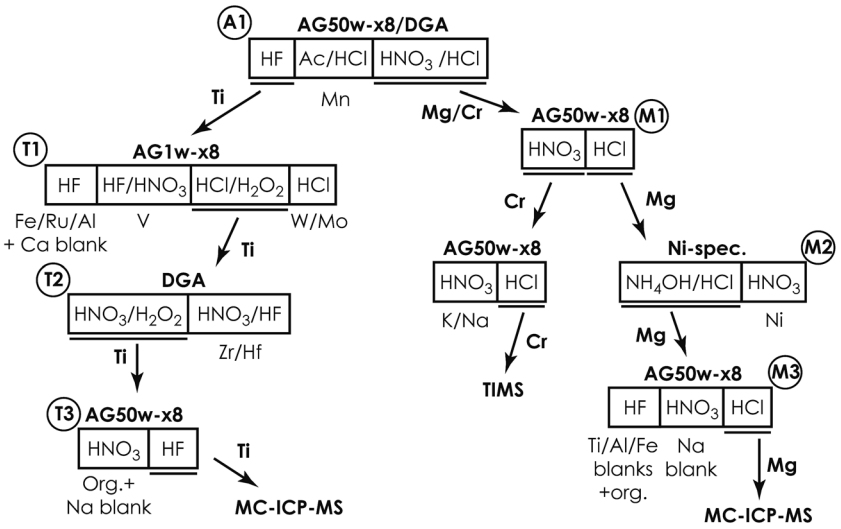

Fig. 1 Schematic diagram of the multi-element ion chromatographic separation protocol.

through chromatographic Cr purification.[22] Thus, to speciate >97% of the Cr into the $Cr(H_2O)_6^{3+}$ form characterized by a high affinity for the cation resin, we used a sample pre-treatment procedure involving dissolution in 2 M HNO_3 followed by dilution and equilibration in 0.5 ml of 0.5 M HNO_3 + 3 wt% H_2O_2 for 5–7 days at room temperature according to procedures described in Larsen *et al.* 2016.[22] This allows for retention and subsequent elution of Cr together with Mg, resulting in >97% Cr recovery from the first column. To ensure high Ti solubility in the sample load, 0.01 M HF was added to this mixture before equilibration.

1st column (A1). The initial column separates Ti from Mg and Cr (Fig. 1) using a Savillex PFA high-resolution column (ID = 3.2 mm, ID = inner diameter) packed with 640 μl of AG50w-x8 200–400 mesh (Bio-Rad Laboratories) cation exchange resin at a resin-filled column length of 80 mm (in 0.5 M HNO_3) (Table 1, Fig. 2a). Prior to sample loading, the resin was cleaned in ~7 M HNO_3, 1 M HF, and MilliQ water, followed by ~6 M HCl and distilled MilliQ water. To ensure sufficiently low impurity contributions from the resin, we dried down and screened the last 0.5 ml of cleaning 6 M HCl eluted from all columns for possible contaminants using an XSeries ICP-MS. The resin blank contributions were in all cases <0.5 ng Mg, <0.1 ng Ti, and <0.3 ng Cr. The resin was subsequently pre-conditioned in 0.5 M HNO_3 in preparation for sample loading.

After the 5–7 day equilibration procedure described above, the sample was loaded directly onto the column in 0.5 M HNO_3 + 3 wt% H_2O_2 + 0.01 M HF. Titanium was subsequently collected together with Fe, Al, V, Re, W and Mo by elution in 4 ml of 1 M HF (Table 1). This was followed by Mn elution using a 95% acetone + 0.5 M HCl mixture.[24] Calcium was finally separated from the residual sample matrix by unloading Mg, Ca, Ni, Cr, Na and K from the cation exchanger using 10 ml of 3 M HNO_3 and eluting directly onto a pre-cleaned faster-flowing Bio-Rad column containing 0.7 ml DGA-N (TrisKem) resin. The high affinity of Ca for the DGA resin in 3 M HNO_3 (ref. 25) ensures its efficient separation from Mg, Cr, Ni, Na and K, which is collected for further purification. The pore-volumes of DGA and AG50w-x8 resin were subsequently emptied into the collected aliquot using 2 ml of 1 M HNO_3 and 3 ml of 6 M HCl, respectively. Calcium can be unloaded from the DGA column using a few column volumes of 0.001 M HCl. Alternatively, Ca can be cleaned up in a separate step by eluting Mg, Na, K, Cr and Ni together with Ca from the cation exchanger in 4 ml of 6 M HCl (instead of 3 M HNO_3 elution directly onto DGA) and later eluting Mg, Na, K, Cr and Ni through a 0.5 ml DGA column in 5 ml of 1 M HNO_3, while efficiently retaining Ca. Chromatographic recoveries from this 1st column, as asserted on elution aliquots around the collected Ti and Mg/Cr cuts for different types of sample matrices (including BHVO-2, BIR-1, BCR-2, chondrites (CCs & OCs) and CAIs), were >99% for Ti and Cr and >99.95% for Mg.

2nd Mg/Cr column (M1). The second step in the Mg/Cr separation reuses the resin and column from the first step after conditioning of the resin bed. Samples were converted to the Cl form by using two consecutive dissolution–evaporation cycles in 6 M HCl. This time we employed a sample pre-treatment procedure which promotes the formation of neutral, mono- and divalent Cr(III)–Cl complexes with low cation exchanger selectivities, thereby allowing for efficient elution of Cr (>97.5%) from the column.[22] This speciation was ensured by sample exposure to 10 M HCl on a hotplate at 130 °C for ~1 day. To effectively minimize any back-reaction of the Cr species to its $Cr(H_2O)_6^{3+}$ form prior to column loading, this 10 M HCl sample aliquot was allowed to cool down for no more than 10 minutes and diluted to 0.5 M HCl using cold (about 5 °C) distilled MQ water. The sample was subsequently loaded onto the column at room temperature. Cr (in the form of Cr(III)–Cl complexes) was then unloaded from the column together with Na and K in 15 ml of 0.5 M HNO_3 (Table 1, Fig. 2b). The residual sample matrix, consisting of Mg and Ni, was eluted in 4 ml of 6 M HCl in which elution tests showed that >99.9% of the Mg is collected in the 1st ml of 6 M HCl eluant. To ensure a robust elution sequence, this separation step was designed such that Mg is

Table 1 Mg/Cr purification protocol

	Elutants	Volume [ml]	Procedures and eluted elements	
Step 1: Ti separation from Mg/Cr + matrix				
AG50w:	7 M HNO_3	3		
	1 M HF	3		
	MilliQ H_2O	2	Cleaning	
	6 M HCl	8		
	MilliQ H_2O	2		
	0.5 M HNO_3	2	Conditioning	
	Load in 0.5 M HNO_3 + 0.01 M HF + 3 wt% H_2O_2	0.5	Smp loading + Ti, Al, Fe, V	Collect Ti
	1 M HF	4	Ti, Al, Fe, V, W, Hf, Mo, Zr, Ru	
	MilliQ H_2O	0.5		
	95% Ac + 0.5 M HCl	2.5	Mn	
	MilliQ H_2O	1		
DGA-N (or 6 M HCl unload from AG50w-x8 + separate DGA Ca-cleanup w/1 M HNO_3):				
	0.001 M HCl	8	Cleaning	
	MilliQ H_2O	5		
	3 M HNO_3	2	Conditioning	
	3 M HNO_3 elute from AG50 onto DGA	10		Collect Mg/Cr
	1 M HNO_3 unload from DGA	2	Mg, Cr, Ni, Na, K	
	6 M HCl unload from AG50	3		
	0.001 M HCl DGA unload (optional)	10	Ca	
Step 2: Mg and Cr separation				
AG50w:	0.5 M HCl	2	Conditioning	
	Load in 0.5 M HCl	5	Smp loading	Collect Cr
	0.5 M HNO_3	12	Cr, Na, K	
	MilliQ H_2O	0.5		
	6 M HCl	4	Mg, Ni	Collect Mg
Step 3: Ni clean-up				
Ni-spec:	MilliQ H_2O	1	Cleaning	
	0.2 M NH_4OH + 0.1 M HCl	6	Conditioning + cleaning	
	Load in 0.2 M NH_4OH + 0.1 M HCl	1.5	Smp loading + Mg	Collect Mg
	0.2 M NH_4OH + 0.1 M HCl	5	Mg	
	3 M HNO_3 unload (optional)	2	Ni	
Step 4: Final Mg purification				
AG50w:	0.5 M HCl	0.3	Conditioning	
	Load 0.5 M HCl	0.3	Smp loading	
	1 M HF	0.3	Ti, Al, Fe blk	
	0.5 M HNO_3	1	Org., anions, Na blk	
	MilliQ H_2O	0.1		
	6M HCl	0.65	Mg	Collect Mg

Step	Resin	Volume [ml]	Column
1 + 2	AG50w-x8 200–400 mesh, Biorad Lab.	0.64	Savillex; ID = 3.2 mm, length = 80 mm
1	DGA normal, 50–100 μm, Triskem	1.0	Pasteur pipette; ID = 5.8 mm, length = 38 mm
3	Ni-spec resin, Triskem	0.26	Pasteur pipette; ID = 3.5 mm, length = 27 mm
4	AG50w-x8 200–400 mesh, Biorad Lab.	0.1	Savillex; ID = 1.6 mm, length = 50 mm

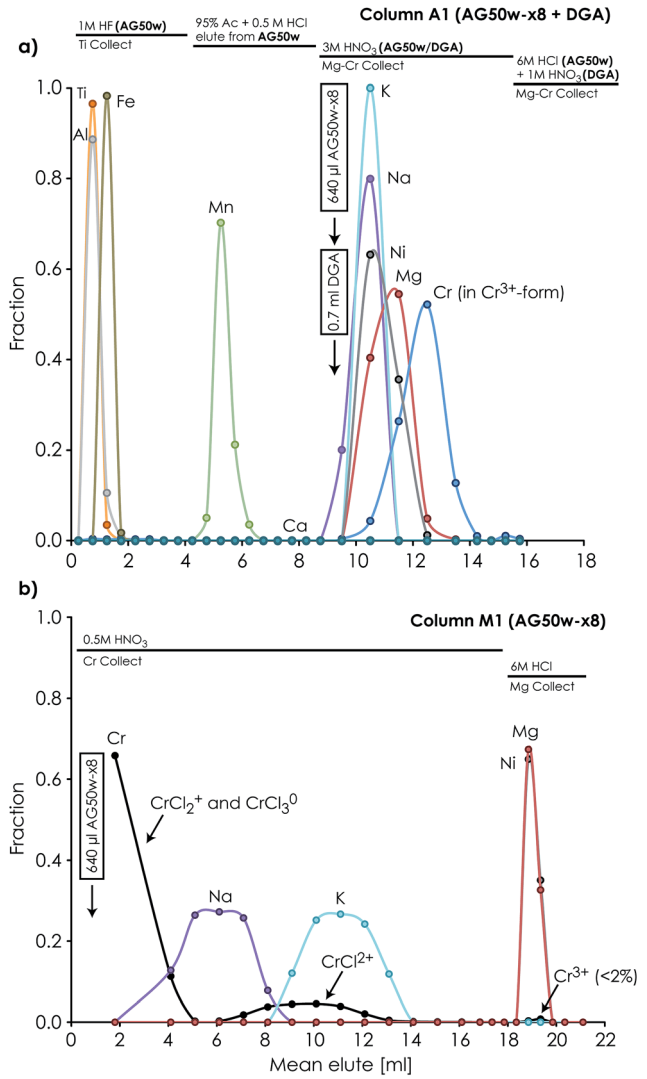

Fig. 2 Ion chromatographic elution profiles of elements separated on (a) the 1st separation column (A1) using a cation exchanger (AG50w-x8 200–400 mesh, ID = 3.2 mm, L = 80 mm) for eluting Al, Ti, Fe and Mn, followed by Mg, Cr, Ni, Na, K and Ca elution onto a faster-flowing DGA-N (50–100 µm) resin-filled anion exchange column, which retains Ca while eluting the other elements and (b) the 2nd Mg/Cr separation column (M1), which separates Cr (together with Na and K) from Mg and Ni by reusing the cation exchange column in A1.

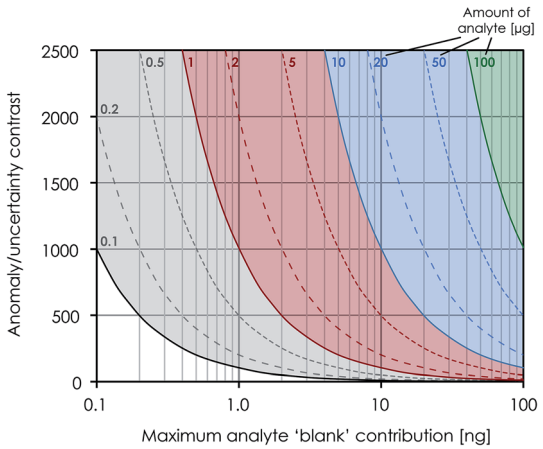

Fig. 3 Diagram showing the effect that impurity contribution (known as 'blanks' with isotopically normal composition) from chemical purification of an analyte has on the maximum isotope anomaly, which can be accurately determined within the stated uncertainty. For example, a procedural Ti 'blank' contribution of 0.8 ng introduced into a 1 µg Ti sample through chemical purification provides an anomaly/uncertainty contrast of 1250. With a stated external reproducibility of 12 ppm for μ^{50}Ti*, this allows for the accurate analysis of materials with anomalies in μ^{50}Ti* of up to 15 000 ppm.

retained even with an additional >50% of the volume of 0.5 M HNO_3 loaded onto the column. Thus, the procedure ensures >99.99% recovery of Mg and >98% Cr recovery from this column. Cr can be further purified from Na and K using a sample pre-treatment procedure involving 5–7 day equilibration in 0.5 ml of 0.5 M HNO_3 + 3 wt% H_2O_2 at room temperature in order to speciate >97% of the Cr into its $Cr(H_2O)_6^{3+}$ form. The sample can then be loaded onto a miniaturized 260 µl AG50-x8 200–400 mesh (Bio-Rad) cation exchange column (ID = 3.5 mm; length = 27 mm), and Na and K were eluted using 6 ml of 0.5 M HNO_3, followed by collection of Cr in 3 ml of 6 M HCl (Fig. 1). The Cr pre-treatment procedure and the cation exchange step may be repeated on the Na/K elution cut in order to recover the last 3% Cr. This approach should result in a total Cr recovery of >94%, thereby avoiding significant mass-dependent isotope fractionation effects.[22]

3rd Mg column (M2). The third Mg purification column involves in the separation of Ni using 260 µl of Ni specific resin (TrisKem) loaded onto a custom-made column made from Pasteur pipettes with an inner diameter of 3.5 mm (Table 1). The Mg/Ni aliquot from the preceding column was converted to the Cl form by using two consecutive dissolution–evaporation cycles in 6 M HCl, redissolved in 0.5 M HCl on a hotplate to ensure complete dissolution and subsequently diluted to 0.1 M HCl using NH_4OH and distilled MilliQ water to obtain a 1.5 ml loading solution of 0.2 M NH_4OH + 0.1 M HCl at pH > 9. This alkaline solution allows the complexation of Ni with dimethylglyoxime (DMG) bound to the resin, which would otherwise be irreversibly destroyed by reaction with H^+ in acidic solutions. Magnesium was loaded onto the column and collected in 5 ml of 0.2 M NH_4OH + 0.1 M HCl. Following this separation procedure, NH_4 salts were destroyed by sample exposure to HCl/HNO_3(3 : 1) on a hotplate at 130 °C and subsequently converted to the Cl form using ~6 M HCl in preparation for the final Mg purification step. The resin-bound Ni–DMG complex can be destroyed and Ni can be eluted with a few column volumes of an acidic solution, such as 2 M HNO_3. The chromatographic Mg recoveries from this column were >99.99%.

4th (final) Mg column (M3). Magnesium was finally purified from residual organics introduced during chromatography that may generate drift and signal spikes during data acquisition using MC-ICP-MS. To this effect, samples were loaded in 300 µl of 0.5 M HCl on a pre-cleaned 100 µl AG50w-x8 200–400 mesh (Bio-Rad) resin-filled Savillex micro-column (ID = 1.6 mm; length = 50 mm) (Table 1). Organics, together with potential Al,

Table 2 Ti purification protocol

	Elutants	Volume [ml]	Procedures and eluted elements	
Step 1: same as Step 1 in Table 1				
Step 2: Ti (+Zr,Hf) separation from Al, Fe, V, Ru, Mo, W				
AG1:	1 M HF + 0.2 M HNO_3	3		
	3 M HCl + 0.03 wt% H_2O_2	3	Cleaning	
	Dil. HCl	4		
	MilliQ H_2O	2		
	1 M HF + 0.2 M HNO_3	3	Conditioning	
	Load in 1 M HF + 0.2 M HNO_3	0.4	Smp loading + Fe, Al, V, Ru	
	3 M HF	3	Fe, Al, V, Ru (+Ca + Cr blank)	
	1 M HF + 0.2 M HNO_3	6	V	
	3 M HCl + 0.03 wt% H_2O_2	**3**	**Ti, Zr, Hf**	**Collect Ti**
	0.5 M HCl unload (optional)	7	Mo, W	
Step 3: Ti separation from Zr (+Hf)				
DGA:	0.001 M HCl	3	Cleaning	
	MilliQ H_2O	2	Cleaning	
	1 M HNO_3 + 0.5 wt% H_2O_2	3	Conditioning + cleaning	
	Load in 1 M HNO_3 + 0.5 wt% H_2O_2	**0.4**	**Sample loading**	**Collect Ti**
	1 M HNO_3 + 0.5 wt% H_2O_2	**5**	**Ti (Ca blk retained)**	
	1 M HNO_3 + 1 M HF (optional)	5	Elute Zr, Hf	
Step 4: Final Ti purification				
AG50w:	6 M HCl	2	Cleaning	
	MilliQ H_2O	1	Cleaning	
	0.5 M HNO_3	0.3	Conditioning	
	Load in 0.5 M HNO_3	0.3	Smp loading + Org. + Na blk	
	0.5 M HNO_3	1	Organics + Na blk	
	0.1 M HF	**1**	**Ti (Ca, Cr, Fe blks retained)**	**Collect Ti**

Step	Resin	Volume [ml]	Column
1	AG50w-x8 200–400 mesh, Biorad Lab.	0.64	Savillex; ID = 3.2 mm, length = 80 mm
1	DGA normal, 50–100 μm, Triskem	1	Pasteur pipette; ID = 5.8 mm, length = 38 mm
2	AG1-x8 200–400 mesh, Biorad Lab.	0.60	Pasteur pipette; ID = 3.5 mm, length = 62 mm
3	DGA normal, 50–100 μm, Triskem	0.26	Pasteur pipette; ID = 3.5 mm, length = 27 mm
4	AG50w-x8 200–400 mesh, Biorad Lab.	0.1	Savillex; ID = 1.6 mm, length = 50 mm

Ti, Fe and Na blanks, were eluted from the column in 0.3 ml of 1 M HF followed by 1 ml of 0.5 M HNO_3. The purified Mg fraction was finally collected in 0.65 ml of 6 M HCl and converted to the NO_3 form through two evaporation–dissolution cycles with ~7 M HNO_3 in preparation for mass-spectrometric analysis using MC-ICP-MS. Magnesium recoveries from this column were >99.99%, thereby ensuring a final chromatographic Mg recovery of >99.9%. Total procedural blanks were

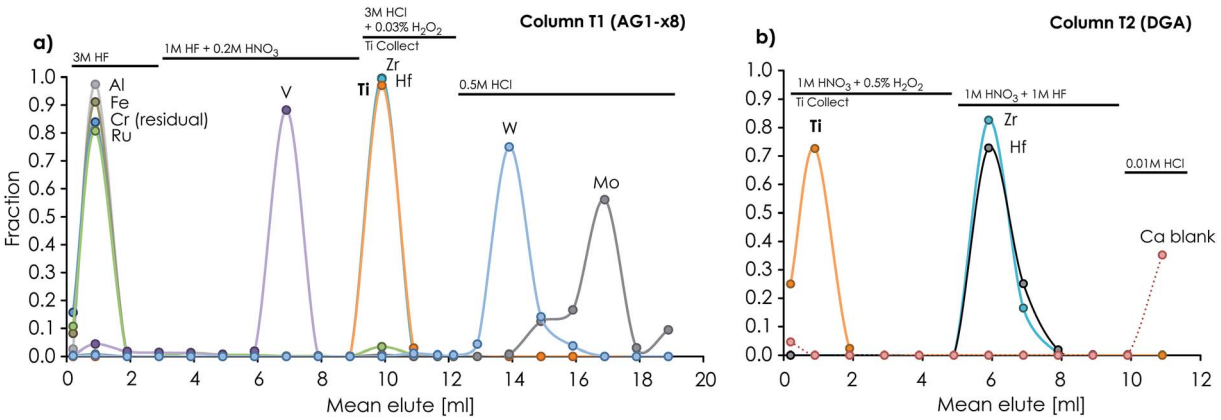

Fig. 4 Ion chromatographic elution profiles of elements separated on (a) the anion exchanger (600 μl AG1-x8 200–400 mesh) column T1 (ID = 3.5 mm, L = 62 mm), which separates Ti (together with Zr and Hf) from Al, Fe, Ru, V, W and Mo, and (b) the 3rd Ti purification column (T2, ID = 3.5 mm, L = 27 mm) packed with 250 μl of DGA-N 50–100 μm resin.

typically <5 ng (n = 29), which is insignificant compared to the amount of Mg processed through the columns (~5 μg). We note that with a reproducibility of 4.1 ppm for μ^{26}Mg*, such a low blank level allows for accurate analysis of materials with μ^{26}Mg* anomalies up to 4100 ppm (Fig. 3), *i.e.* about 4 times more anomalous than most CAIs (μ^{26}Mg* ~ 1000 ppm) and well within the range of most solar system materials, as well as the rare and extremely anomalous FUN (Fractionation and Unidentified Nuclear effects, μ^{26}Mg* down to ~−2000 ppm) CAIs found in primitive meteorites.

2nd Ti column (T1). Titanium (together with Zr and Hf) was separated from Al, Fe, V, Ru, Mo and W on a pre-cleaned 600 μl AG1-x8 200–400 mesh (Bio-Rad) anion exchange column (ID = 3.5 mm; length = 62 mm) (Table 2, Fig. 4a). The sample was loaded in 0.4 ml of 1 M HF + 0.2 M HNO_3 and Al, Fe, and Ru (and some V) were eluted in 3 ml of 3 M HF, followed by V elution in 6 ml of 1 M HF + 0.2 M HNO_3. Titanium (incl. Zr and Hf) was subsequently collected using 3 ml of 3 M HCl + 0.03 wt% H_2O_2 and converted to the NO_3 form using ~7 M HNO_3. When drying down from 3 M HCl, care was taken not to exceed 110 °C, thereby avoiding the loss of Ti in the form of $TiCl_4$ (boiling temperature of 136 °C (ref. 26)). Chromatographic Ti recoveries from this column were >99.3%, as asserted on >40 samples.

3rd Ti column (T2). Titanium was then separated from Zr and Hf (and potential Ca blanks introduced through the chemistry) using a pre-cleaned 260 μl DGA-N (50–100 μm, TrisKem) column (ID = 3.5 mm; length = 27 mm) (Table 2, Fig. 4b). The sample is loaded in 0.4 ml of 1 M HNO_3 + 0.5 wt% H_2O_2 and collected in another 5 ml of 1 M HNO_3 + 0.5 wt% H_2O_2. In preparation for the final purification step, the sample was subsequently subjected to three evaporation–dissolution cycles in ~7 M HNO_3 to make sure that only trace H_2O_2 was present in the loading solution, which is known to reduce the selectivity of the cation exchanger for Ti through the formation of anionic species. Chromatographic Ti recoveries from this column were >99.7%.

4th (final) Ti column (T3). Titanium was finally purified from potential organics and Ca and Cr blanks introduced into the sample during chromatography using the same type of pre-cleaned micro-column as that used for the final Mg purification step (Savillex column (ID = 1.6 mm; length = 50 mm) containing 100 μl AG50w-x8 200–400 mesh, Bio-Rad) (Table 2). The samples were loaded in 300 μl of 0.5 M HNO_3 after which organics and residual Na were eluted with another 1 ml of 0.5 M HNO_3. Titanium was finally collected and separated from potential Ca, Cr and Fe blanks using 1 ml of 0.1 M HF. The purified Ti was then converted to the NO_3 form through three evaporation–dissolution cycles in ~7 M HNO_3 in order to sufficiently reduce the HF concentration in preparation for isotope analysis using MC-ICP-MS. Titanium recoveries from this column were >99.2%, thereby ensuring a final chromatographic Ti recovery of >97%. Total procedural blanks were typically <0.8 ng Ti (n = 12), which is insignificant compared to the amount of Ti processed through the columns (~1 μg). The

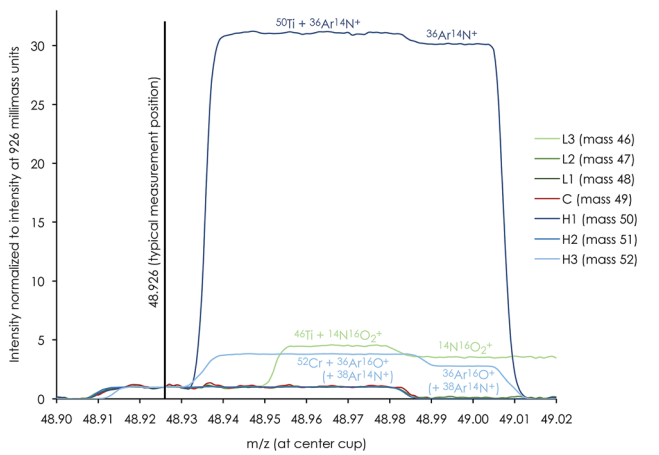

Fig. 5 Mass peak scan profile of a dilute (0.1 ppb) mixture of Ti, V and Cr demonstrating that gas-based molecular interference from $^{36}Ar^{14}N^+$ on ^{50}Ti, $^{14}N^{16}O_2^+$ on ^{46}Ti and $^{36}Ar^{16}O^+$ (+$^{38}Ar^{14}N^+$) on ^{52}Cr is clearly resolved from the typical measurement position at X.926 in high-resolution mode. The abundances of other potential molecular interference on the other titanium isotopes (^{47}Ti, ^{48}Ti and ^{49}Ti) and ^{51}V are negligible.

Table 3 Isotopes of interest for Ti isotope analysis using MC-ICP-MS and Faraday cup configuration. Numbers in parentheses are the millimass unit offset of molecular interference peaks relative to the corresponding isotope of interest, *i.e.* ^{44}Ca, ^{46}Ti, ^{47}Ti, ^{48}Ti, ^{49}Ti, ^{50}Ti, ^{51}V or ^{52}Cr. Major molecular interferents are marked in bold

Ti isotopes			46	47	48	49	50		
Direct isobaric interferences									
Ca		44	46		48				
V							50	51	
Cr							50		52
Potential molecular interferences									
Argides (Ar)		^{40}Ar^{4}He (10)			^{36}Ar^{12}C^{+} (20)	^{36}Ar^{13}C^{+} (23), ^{36}Ar^{12}C^{1}H^{+} (28)	**^{36}Ar^{14}N^{+} (26)**	^{38}Ar^{13}C^{+} (22), ^{36}Ar^{15}N^{+} (24), ^{36}Ar^{14}N^{1}H^{+} (34)	^{40}Ar^{12}C^{+} (22), **^{36}Ar^{16}O^{+} (22)**, **^{38}Ar^{14}N^{+} (25)**
Flourides (F)				^{28}Si^{19}F^{+} (24)					
Other carbides (C)				^{12}C^{35}Cl^{+} (17)	^{12}C^{4+} (52)	^{12}C^{37}Cl^{+} (18)			
Other chlorides (Cl)						^{35}Cl^{14}N^{+} (24)	^{35}Cl^{15}N^{+} (24), ^{1}H^{14}N^{35}Cl^{+} (35)	^{36}Cl^{15}N^{+} (24), ^{35}Cl^{16}O^{+} (20)	^{35}Cl^{16}O^{1}H^{+} (31), ^{35}Cl^{17}O^{+} (27)
Other nitrides (N) & oxides (O), *etc.*		**^{14}N$_2$^{16}O^{+} (46)**, ^{30}Si^{14}N^{+} (21)	**^{14}N^{16}O$_2^{+}$ (40)**, ^{15}N$_2$^{16}O^{+} (43), ^{30}Si^{16}O^{+} (16)	^{33}S^{14}N^{+} (23), ^{15}N^{16}O$_2^{+}$ (38), ^{14}N^{16}O$_2$^{1}H^{+} (21)	^{14}N^{16}O^{18}O^{+} (49), ^{14}N^{17}O^{2+} (53)	^{14}N^{17}O$_2$^{1}H^{+} (61)			
		^{22}Ne$_2^{+}$ (27)							
Doubly charged interferences									
Zr			91	92	94	96			
Mo				92	94	96	98	100	
Ru						96	98	100	
Cup configuration									
Line 2 (Ti isotopes + V & Cr)	Cup		L4	L3	L2	L1	C	H1	H2	H3
	Mass		45.5Zr^{2+}	46Ti	47Ti	48Ti	49Ti	50Ti	51V	52Cr
Line 1 (Ca interference)	Cup	L3		L1	C	H1	H2	H3		
	Mass	44Ca		46Ti	47Ti	48Ti	49Ti	50Ti		

reproducibility of 12 ppm in μ^{50}Ti* allows for the accurate analysis of materials with μ^{50}Ti* anomalies up to 15 000 ppm (Fig. 3), *i.e.* well within the range of most solar system materials, including FUN-type CAIs.

3. Mass spectrometry

3.1 Mg isotope analysis using MC-ICP-MS

High-precision Mg isotope analysis was performed using the Thermo-Finnigan Neptune Plus MC-ICP-MS located at the Centre for Star and Planet Formation (Natural History Museum of Denmark, University of Copenhagen), using procedures based on Bizzarro *et al.* 2011.[23] In brief, purified Mg was introduced into the plasma source by means of an Apex IR desolvating nebuliser in a 2% HNO_3 run solution at 50 μl min^{-1} using a Thermo Fisher Jet sample cone and skimmer X-cone interface in high-resolution mode. The typical sensitivity of the instrument was ~200 V ppm^{-1} of ^{24}Mg and samples were typically analysed at ~50 V. Magnesium isotope data were acquired in static mode using three Faraday collectors connected to amplifiers with 10^{11} ohm feedback resistors. Samples and standards were analyzed 10 times with each analysis consisting of 100 cycles of 16.78 second integrations separated by a total of 822 seconds of on-peak zero blank measurements in clean 2% HNO_3 solution.

Corrections for instrumental mass bias were obtained by sample–standard bracketing with sample/standard peak intensities matching to better than 5%. Stable Mg isotope ratios are reported in parts per million (ppm) deviation relative to the composition of the Mg reference standard DTS-2B[27] according to: $\mu^{i}\mathrm{Mg} = [(^{i}\mathrm{Mg}/^{24}\mathrm{Mg})_{\mathrm{sample}}/(^{i}\mathrm{Mg}/^{24}\mathrm{Mg})_{\mathrm{DTS\text{-}2B}} - 1] \times 10^{6}$, where i = 25 or 26. The mass-independent μ^{26}Mg* (radiogenic ingrowth and nucleosynthetic effects) is calculated as the deviations of the corrected ^{26}Mg/^{24}Mg from the reference standard, normalized to ^{25}Mg/^{24}Mg = 0.126896 (ref. 23), assuming that instrumental mass discrimination follows the exponential mass-fractionation law. Data reduction was conducted offline using the freeware software package Iolite.[28]

3.2 Ti isotope analysis using MC-ICP-MS

High-precision Ti isotope analysis was performed by standard–sample–standard bracketing using the Thermo-Finnigan Neptune Plus MC-ICP-MS located at the Centre for Star and Planet Formation (Natural History Museum of Denmark, University of Copenhagen). Following Ti purification, the samples were dissolved in 0.3 M HNO_3 + 0.001 M HF and introduced into the plasma source by means of an Apex HF desolvating nebuliser (with Ar + N_2) at a sample uptake rate of 30–45 μl min^{-1}. To enhance ion transmission and sensitivity, we used a Thermo Fisher Jet sample cone and skimmer X-cone interface. The measurements were performed on the low mass side of peak shoulders. We used high mass resolution mode, defined as mass resolving power > $8000(m/(m_{0.95} - m_{0.05}))$, measured in the center cup. These conditions are sufficient to efficiently filter out slightly heavier polyatomic interference from *e.g.* ^{36}Ar^{14}N^{+} on ^{50}Ti, ^{14}N$_2$^{16}O^{+} or ^{22}Ne^{+} on ^{44}Ca, and ^{40}Ar^{12}C^{+} or ^{36}Ar^{16}O^{+} ($^{+38}$Ar^{14}N^{+}) on ^{52}Cr (shown in Fig. 5 for a 0.1 ppb solution of Ti, V and Cr); see Section 4.4 for detailed discussion on the measurement conditions. For a 250 ppb run solution, this resulted in a typical sensitivity of ~12 V of ^{48}Ti. Standard and sample intensities were matched to within 5% and tune settings were optimized before each analytical session to maximize the sensitivity and signal stability.

Ti isotope data were acquired in dynamic mode by peak jumping using Faraday collectors connected to amplifiers with 10^{11} ohm feedback resistors for ^{46,47,48,49,50}Ti, ^{51}V, ^{52}Cr and ^{44}Ca and a 10^{13} ohm feedback resistor to monitor doubly charged ^{91}Zr^{2+} at half-mass 45.5. Each sequence consisted of a number of repeated measurements on a sample bracketed by standards and blanks, each consisting of one cycle of 33.6 seconds of integration for ^{44}Ca in line 1 followed by 200 cycles of 2.1 seconds of integration for Ti isotopes, ^{51}V and ^{52}Cr in line 2 (Table 3). A peak centering procedure was automatically performed prior to each standard analysis. With a sample uptake time of 100 seconds, this corresponds to a total effective analysis time of 8.9 hours for 10 repeats.

After correction for isobaric interference, stable Ti isotope ratios were calculated as parts per million (ppm) deviation from the composition of the Origins Laboratory Ti reference standard (OL-Ti)[29] according to: $\mu^{i}\mathrm{Ti} = [(^{i}\mathrm{Ti}/^{47}\mathrm{Ti})_{\mathrm{sample}}/(^{i}\mathrm{Ti}/^{47}\mathrm{Ti})_{\mathrm{OL\text{-}Ti}} - 1] \times 10^{6}$, where i = 46, 48, 49 or 50. The mass-independent μ^{46}Ti*, μ^{48}Ti*, μ^{49}Ti* and μ^{50}Ti* components represent deviations in part per million (ppm) from the bracketing standard, OL-Ti, after correction for mass-dependent fractionation by internal normalization to either ^{49}Ti/^{47}Ti = 0.749766 or ^{48}Ti/^{47}Ti = 10.070565 using the exponential mass-fractionation law.[10,18,30,31] Data reduction was conducted offline using the freeware software package Iolite.[28]

4. Results and discussion

4.1 Minimizing procedural blanks and optimizing the performance of chromatographic procedures

Due to potential matrix effects and isobaric interferences, isotope analysis by MC-ICP-MS requires sufficient ion exchange chromatographic purification of analytes to ensure measurement accuracy.[32] The need for such chemical processing of samples prior to data acquisition, however, unavoidably results in small impurity contributions, known as 'blanks', introduced either through (1) release from the ion exchange resins, (2) the chemical reagents used for sample digestion and during chromatographic purification, or (3) other exogenous contributions introduced during sample handling. Blanks introduced through chromatographic purification can potentially dilute the true isotopic signature of the 'purified' element and thus generate false results. This delicate balance between chemical purification and blank contributions becomes increasingly important when handling samples that are highly isotopically anomalous. This is because of the large isotopic contrast between the sample and typical 'Earth'-like blanks. Amongst some of the most isotopically anomalous samples are the first solids known to have formed in our solar system, namely Ca–Al-rich inclusions (CAIs) in primitive chondritic meteorites. These

inclusions commonly exhibit large mass-dependent and/or mass-independent anomalies in the permil range in a wide range of elements and thus contain important isotopic fingerprints of the very earliest evolution of our solar system.[10,15,33–37] As such, the chemical and analytical procedures described here were optimized to obtain accurate and precise isotope data from isotopically anomalous materials.

Taking advantage of the increased precision of modern mass spectrometric techniques and thus the small amount of sample that can be precisely analysed simultaneously requires sufficient reduction of procedural blanks introduced through chemical processing. Minimizing procedural blanks demands a sufficient reduction in the amount of resins and acid used through chromatographic purification. Thus, in order to ensure effective separation of most of the sample matrix during the first purification step, the first column ensures a removal of >75% of matrix elements (Fe, Al, Ti, Ca, V and Mn) from Mg and Cr for a variety of rock samples (Table S1†). Ti is effectively separated from the residual matrix in its 2nd purification step, requiring subsequent removal of only Zr. This effectively minimizes the amount of resins and reagents required in the subsequent purification steps, thereby reducing major blank contributions.

The separation of Mg from elements that may generate doubly charged interference (*e.g.* $^{48}Ca^{2+}$, $^{48}Ti^{2+}$, $^{50}Ti^{2+}$, $^{50}V^{2+}$, $^{50}Cr^{2+}$ and $^{52}Cr^{2+}$) and/or affect the instrumental mass bias of the sample as compared to the bracketing standard during analysis (*e.g.* Al, Fe, Na, Ni, Mn and Ca) is critical for reliable and accurate Mg isotope measurements using MC-ICP-MS.[23,38] Ca is specifically known to be problematic for isotope analysis of meteoritic materials, as it may induce significant isobaric interference on mass 24 from doubly charged ^{48}Ca and can result in apparent $\mu^{26}Mg^*$ anomalies.[32,38] Thus, in handling sample matrices with high Ca levels compared to Mg, such as CAIs, efficient separation of Ca from Mg is important. Cation to Mg ratios were monitored in purified samples processed through the chromatographic separation protocol and found to be <~0.001 (examples are given in Table S1†).

Accurate and precise mass spectrometric analysis of Ti is further compromised by direct isobaric interference from Ca (on masses 46 ($^{46}Ca \sim 0.004\%$) and 48 ($^{48}Ca \sim 0.187\%$)), V (on mass 50 ($^{50}V \sim 0.2497\%$)) and Cr (on mass 50 ($^{50}Cr \sim 4.3452\%$)) and potential doubly charged interference from Zr (on masses 46, 47 and 48), Mo (on all Ti isotopes) and Ru (on masses 48, 49 and 50) (Table 3). Therefore, the chromatographic purification procedure was designed to ensure sufficient separation of these elements from Ti. However, Ca blanks may be especially problematic, since Ca can be introduced through general sample handling from gloves and pipette tips. Thus, all chromatographic columns used in the purification of Ti were designed to separate potential Ca blanks introduced on the sample from Ti. The last column further ensures the effective separation of potential Ca and Cr blanks from the purified Ti fraction. Moreover, all reagents used in the chromatographic chemistry, as well as analytical solutions, were blank tested in order to ensure a sufficiently low Ca blank introduced on the samples. Finally, to eliminate potential interference from chlorides ($^{35}Cl^{14}N^+$ on ^{49}Ti, $^{35}Cl^{15}N^+$ and $^1H^{14}N^{35}Cl^+$ on ^{50}Ti, $^{36}Cl^{15}N^+$ and $^{35}Cl^{16}O^+$ on ^{51}V and $^{35}Cl^{16}O^1H^+$ and $^{35}Cl^{17}O^+$ on ^{52}Cr), HCl-based reagents were avoided on the last two columns.

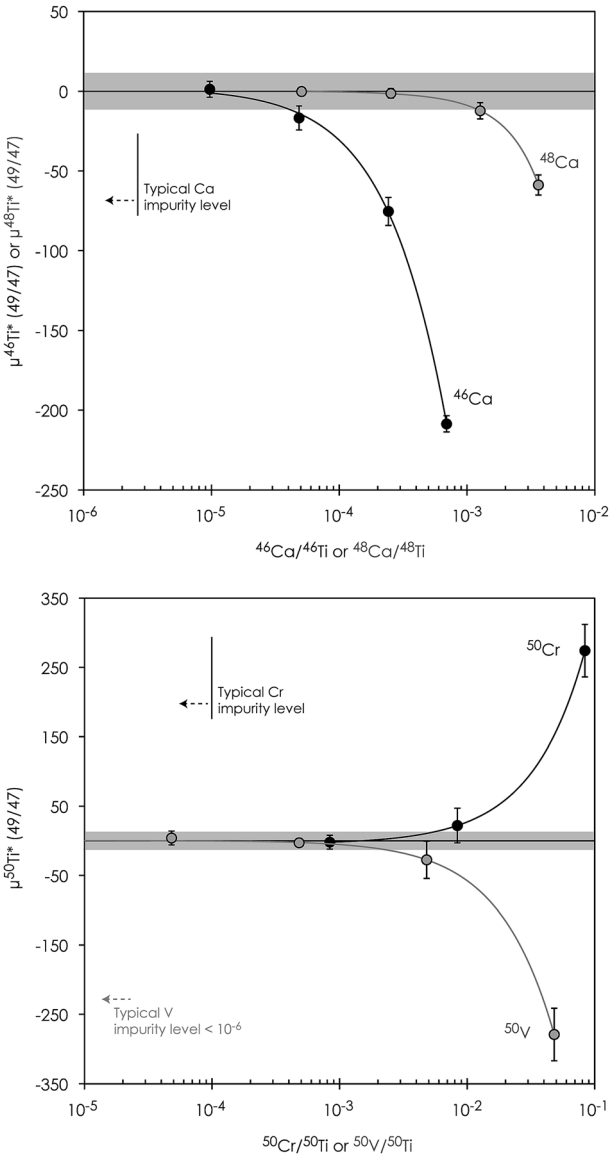

Fig. 6 Titanium isotope composition of a Ca-, V- and Cr-doped Alfa Aesar Ti standard solution after interference correction showing their impact on the accuracy of Ti isotope measurements. Grey shaded regions represent the external reproducibility (2sd) on $\mu^{46}Ti^*$, $\mu^{46}Ti^*$ and $\mu^{46}Ti^*$ as asserted on repeated measurements on the Allende CV CAI 'A3'. Error bars represent the 2se external error in individual runs.

4.2 Efficiency of the multi-element ion chromatographic separation protocol

Our protocol allows for the efficient separation of multiple elements from the same sample aliquots (Fig. 1). Fig. 2 and 4 show the high resolution achieved for individual elution peaks as exemplified by a synthetic CAI composition. The elution profiles of other types of sample matrices (including a dunite (DTS-2B), basalt (BIR-1), lherzolite (J11), ordinary chondrite (Tennasilm),

Table 4 Doping tests on a pure Alfa Aesar Ti standard for uncorrected interference from Zr, Mo and Ru. The bracketing standard was an undoped aliquot of the Alfa Aesar Ti standard

Atomic ratio	μ^{49}Ti	μ^{46}Ti* (49/47)	μ^{48}Ti* (49/47)	μ^{49}Ti* (48/47)	μ^{50}Ti* (49/47)	N[a]
Zr/Ti = 0.002	7 ± 63	1.3 ± 8.1	−0.6 ± 3.5	1.3 ± 7.0	−5.8 ± 4.3	3
Zr/Ti = 0.0005	11 ± 23	10.0 ± 10.0	−1.8 ± 3.3	3.6 ± 6.5	−14.0 ± 11.0	7
Mo/Ti = 0.01	29 ± 33	19.0 ± 21.0	−0.2 ± 5.7	0.0 ± 11.0	−12.6 ± 8.2	3
Mo/Ti = 0.001	1 ± 19	−5.8 ± 6.6	−0.6 ± 5.3	1.0 ± 10.0	−0.1 ± 8.4	10
Ru/Ti = 0.001	2 ± 16	−4.8 ± 9.0	−1.1 ± 3.0	2.2 ± 5.9	−5.5 ± 7.5	10

[a] Number of repeated measurements.

a CAI, and synthetic mixtures) were equally well resolved, demonstrating the reproducibility and efficiency of the chromatographic procedures in separating multiple elements from various types of sample matrices. The efficiency of the chromatographic protocol in separating elements other than Mg, Ti and Cr was evaluated by measuring K, Ca, V, Fe, Ni, Zr, Mo, Ru, Hf, and W eluted from the respective columns. Their recoveries were found to be near 100% for K, Ca, V, Fe, Ni, Zr, Mo, Hf and W, and >92% for Ru in their respective collection aliquots (Tables 1 and 2). The lower recovery of Ru most likely results from complications associated with chemical speciation and redox conditions in the eluting acid, thereby distributing Ru species with variable selectivity over the column. Prior to future isotope work on these elements, their purity in the collected aliquots needs to be addressed and further purification for some is required.

4.3 Accuracy and reproducibility of Mg isotope measurements

The procedures described here for Mg purification and analysis are optimized to handle considerably smaller samples than previous high-precision Mg isotope protocols,[23] *i.e.* 20 times less. This is attained by minimizing the amount of resin and reagents used in the chemical processing of the sample and optimizing the chromatographic separation scheme, as well as by taking advantage of the Jet and X cone interface. Our results show that isotopically anomalous samples, such as CAIs, can be routinely analysed to an external long-term reproducibility for their stable Mg isotope composition of ±61 ppm (2sd) on μ^{25}Mg and ±4.1 ppm for the mass-independent μ^{26}Mg* component (Table 5). This is comparable to, although less precise, the protocols designed for high-precision Mg isotope analysis of larger samples.[23] The typical internal standard error in each repeated measurement was on the order of 5–15 ppm for μ^{25}Mg and 4–6 ppm for μ^{26}Mg*, whereas the external precision (2se) for 10 repeated measurements on the same aliquot was on the order of 3–10 ppm for μ^{25}Mg and 2–5 ppm for μ^{26}Mg*. This level of precision is adequate to resolve the often very large isotope differences (a few ‰) between refractory inclusions, such as AOAs and CAIs, in primitive meteorites.[15,33,34] 5 μg Mg typically consumed during a full analysis corresponds to the amount of Mg typically found in a spherical CAI of about 350 μm in diameter. This allows for the measurement of the Mg isotope

Table 5 Mg isotope data summary. The bracketing standard was DTS-2B

Sample	Type of material	μ^{25}Mg	μ^{26}Mg*	N[a]
Terrestrial rock standards and samples				
J11(1)	Olivine separated from spinel lherzolite	−13 ± 4	−1.1 ± 5.5	10
J11(2)	Olivine separated from spinel lherzolite	−19 ± 19	−4.3 ± 4.2	10
BIR-1	Icelandic basalt, USGS rock standard	33 ± 4	−0.4 ± 2.4	10
BCR-2	Basalt, Columbia River, USGS rock standard	0 ± 3	−1.3 ± 1.3	10
Meteoritic samples				
Ivuna	CI chondrite	12 ± 5	4.2 ± 2.1	10
Allende	$CV3_{ox}$ chondrite	1 ± 8	10.4 ± 3.1	10
Alfianello	Ordinary chondrite (L6)	25 ± 3	−4.0 ± 2.6	10
Tennasilm	Ordinary chondrite (L4)	4 ± 26	−4.3 ± 1.3	10
NWA 6043	CR2 chondrite	14 ± 4	−4.6 ± 2.2	10
31E	CAI from Efremovka ($CV3_{red}$)	6050 ± 7	1166.2 ± 4.2	10
Reproducibility test				
A3 (1)	CAI from Allende ($CV3_{ox}$)	−1486 ± 8	1321.2 ± 4.9	10
A3 (2)		−1512 ± 10	1323.5 ± 2.7	10
A3 (3)		−1501 ± 10	1321.0 ± 3.8	10
A3 (4)		−1442 ± 3	1318.5 ± 4.6	10
Average and 2sd		***−1485 ± 61***	***1321.1 ± 4.1***	

[a] Number of repeated measurements.

composition of inclusions in non-CV carbonaceous chondrites, such as CR, CO and CM chondrites, which have previously been inaccessible to high-precision isotope analysis by MC-ICP-MS due to their small sizes.

An external reproducibility of 4.1 ppm on $\mu^{26}Mg^*$ restricts the Mg blank contribution (with $\mu^{26}Mg^* \sim 0$) allowed on a sample with *e.g.* a very extreme anomaly in $\mu^{26}Mg^*$ of 5000 ppm (such as a canonical CV CAI fragment with an anomalously high $^{27}Al/^{24}Mg$ ratio of 13.5) to <1‰. Thus, for typical 5 μg Mg required for high-precision isotope analysis following the present analytical procedures, this corresponds to a maximum blank level of 5 ng Mg (Fig. 3), which is fulfilled by our ion chromatographic procedures.

In addition to the reproducibility test, our analysis shows that three terrestrial rock standards (J11, BIR-1 and BCR-2) are all within the error of the bracketing standard DTS-2B (Table 5). Similarly, measurements on a range of chondritic meteorites (CI, CV, CR and OC) and another CAI (31E) are within the error of other high-precision $\mu^{25}Mg$ and $\mu^{26}Mg^*$ data previously reported in ref. 3, 8, 15 and 39. This demonstrates the accuracy of our methods.

4.4 Optimization of Ti mass-spectrometric analytical protocols

Interference corrections and doping tests. Given that the accuracy and precision of Ti isotope analysis are compromised by direct isobaric interference from $^{46,48}Ca$, ^{50}V and ^{50}Cr, as well as doubly charged interference from $^{92,94,96}Zr$, $^{92,94,96,98,100}Mo$ and $^{96,98,100}Ru$, we monitored ^{44}Ca, ^{51}V and ^{52}Cr in order to correct for direct isobaric interference on masses 46, 48 and 50. Doubly charged interference from $^{92,94,96}Zr$ was further monitored at half-mass 45.5 ($^{91}Zr^{2+}$). Their intensities were subtracted from the intensities of ^{46}Ti, ^{48}Ti and ^{50}Ti isotopes. To test the performance of our interference correction routines and evaluate their influence on our measurements, we performed doping tests on a pure 250 ppb Alfa Aesar Ti standard solution. The doped solutions were analysed for their isotope composition by bracketing against a Ti pure aliquot of the Alfa Aesar Ti solution. The results show that our interference correction routines are sufficient up to a cation/Ti atomic ratio of 0.07 for Ca, 0.04 for V, and 0.005 for Cr (Fig. 6). Further doping tests showed that uncorrected interference from doubly charged Zr, Mo and Ru is insignificant at atomic ratios Zr/Ti < 0.002, Mo/Ti < 0.01 and Ru/Ti < 0.001 (Table 4), *i.e.* comparable to or higher than the ratios found in typical unprocessed CAIs and most types to rocky materials. Residual Zr, Mo and Ru, present in the purified Ti samples, should therefore not affect the measurement accuracy. Measured Ca/Ti, V/Ti and Cr/Ti atomic ratios in

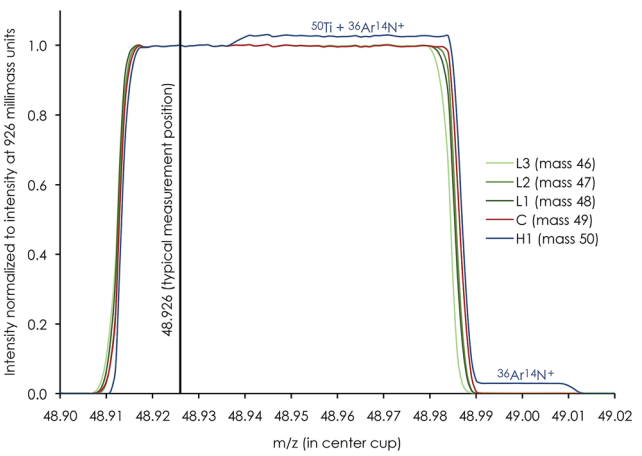

Fig. 7 Mass peak scan profile of a 250 ppb Ti run solution (0.3 M HNO_3 + 0.001 M HF) showing the alignment of individual Ti cups and a sufficiently flat low-mass shoulder plateau of >15 millimass units between peak edges and interference from $^{36}Ar^{14}N^+$ on ^{50}Ti in high-resolution mode. The typical measurement position at X.926 is positioned in the middle of this plateau.

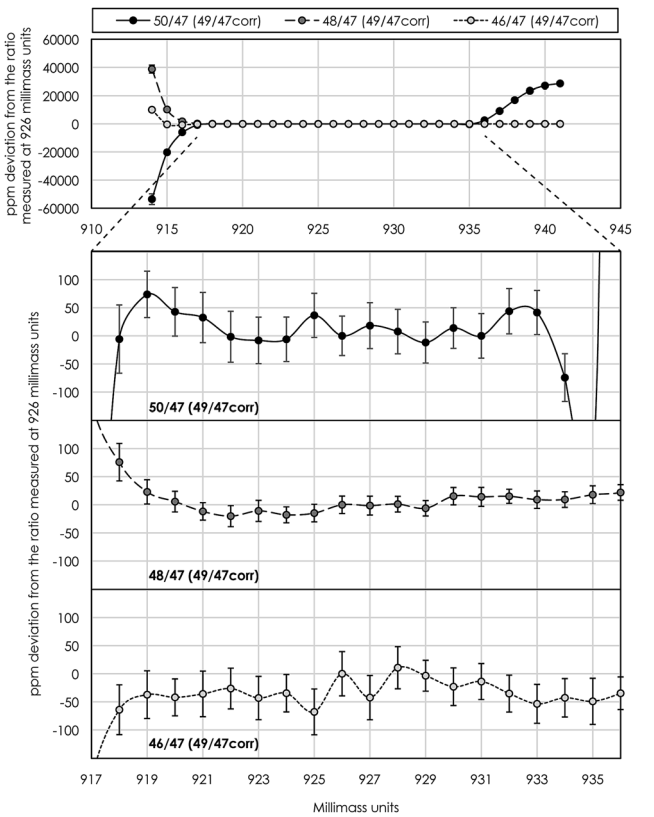

Fig. 8 An example of a 'peak-shoulder-flatness test' used for asserting the mass range on the low-mass side of peaks where the internally $^{49}Ti/^{47}Ti$ normalized mass-fractionation corrected isotope ratios approach constant values, *i.e.* a flat plateau. The typical measurement position at 926 millimass units is in the middle of this flat shoulder plateau, which was acquired by repeated scans over peaks at 8.4 seconds of integration for 1 millimass unit increments from 914 to 941 for a duration of ~15 minutes. Top panel shows the internally normalized mass-fractionation corrected Ti isotope ratios measured over the full mass range. Ratios diverge to extreme values at low-mass peak edges due to small misalignments of individual cups of a few millimass units. The $^{50}Ti/^{47}Ti$ ratio becomes anomalously high at >935 millimass units because of gas-based interference from $^{36}Ar^{14}N^+$ on ^{50}Ti. The three lower panels show the finer details of the flat plateau from 917 to 936 millimass units. This routine was performed prior to each analytical session and the measurement position was adjusted if necessary, thereby ensuring the accuracy, precision and reproducibility of our isotope analysis. Error bars represent the 2se at each mass position.

standards and samples were all insignificant for the precision of our measurements (Table S2†).

Peak-shoulder-flatness test – optimizing measurement position. The accuracy, reproducibility and precision of high-resolution Ti-isotope measurements are strongly dependent on the alignment of detectors and the measurement position on peak shoulders. This is due to the combined effects of magnet drift, tailing from comparatively large interfering molecular interference on the high mass side of Ti peaks, small peak misalignments typically on the scale of a few millimass units, and variations in the peak shape among the detectors used to determine an isotope ratio (Fig. 7). The main analytical challenge is finding a position sufficiently far away from the centre of the peaks to robustly resolve interference, while not moving so far down a peak shoulder that a combination of magnet instabilities and asymmetric decreases in signal intensity compromises the measurement of the isotope ratios of interest. Hence, to ensure a sufficiently flat measurement plateau that minimizes these effects, we performed a series of short-term repeated measurements (each of 8.4 second integrations) interspaced with 1 millimass unit on the low-mass side of peak shoulders before each analytical session. In contrast to traditional peak flatness definitions that describe the effective peak flatness for a single isotope in a single cup, we employ a ratio-based definition that provides a probe of the actual measurement protocols, including a partial data reduction pipeline. The peak-shoulder-flat plateau is defined as the mass range where the internally normalized mass-fractionation corrected isotope ratios approach constant values. Fig. 8 shows an example of such a peak-shoulder-flatness test and the sufficiently flat shoulder plateau around the typical measurement position at X.926 mass units.

Instrumental drift due to magnet instabilities between two peak centers (prior to each standard measurement) was typically less than 1 millimass unit, which is much less than the peak-shoulder-flat plateau of >15 millimass units on the low-mass shoulder. With a typical measurement position in the middle of the shoulder plateau at X.926 mass units, this ensures a flat peak plateau of >7 millimass units on either side of the shoulder measurement position, *i.e.* sufficient to neglect measurement inaccuracy associated with magnet instabilities during an analytical session.

Optimizing Ti analytical protocols. The observation of large-scale μ^{50}Ti* heterogeneity in the solar protoplanetary disk[10] suggests that the Ti isotopic signature of sub-mm-sized disk solids, such as chondrules and CAIs, may provide a tool for disentangling the very earliest processing and transport of material in the solar system. To this effect, and contrary to Trinquier *et al.* 2009 (ref. 10) and Zhang *et al.* 2011 (ref. 18) who positions ^{47}Ti in the central Faraday cup, our cup configuration positions ^{49}Ti in the central Faraday cup. This configuration allows for the optimization of the peak shape for ^{50}Ti in Faraday cup H1, since high mass resolution is generally easier to achieve close to the axial Faraday cup *i.e.* the centre cup for our instrument. This ensures optimal resolution in H1 to robustly resolve $^{36}Ar^{14}N^+$ interference on ^{50}Ti, while at the same time allowing for the $^{36}Ar^{16}O^+$ ($+^{38}Ar^{14}N^+$) interference on the high-mass side of the ^{52}Cr peak to be sufficiently resolved. Using this analytical setup with an integration time of 2.1 seconds in 200 cycles typically resulted in internal standard errors in each repeated measurement of 30–40 ppm for δ^{49}Ti and 25–30 ppm for μ^{50}Ti*. The internal precision (2se) for 10 repeats was typically on the order of 15–30 ppm for δ^{49}Ti and 7–10 ppm for μ^{50}Ti*. The initial tests with longer integration times and fewer cycles (*i.e.* 4.2 seconds × 100 cycles and 8.2 seconds × 50 cycles) had no effect on the internal precision of individual measurements.

Another obstacle towards optimizing measurement precision during Ti isotope analysis in dynamic peak jumping mode is the idle times (prior to actual measurement) needed for amplifiers and magnets to settle when jumping between peaks in two cup configuration lines. Conventional analytical protocols for Ti isotope analysis utilize consecutive peak-jumping between two cup configuration lines for a given number of cycles,[10,18] thereby measuring each line an equal number of times. This approach, however, uses a relatively large volume of sample solution because of the idle time necessary for magnet stabilization between two peak jumps. Our analysis shows that an idle time of at least 3 seconds is required for magnet and amplifier stabilization (Fig. 9). For 200 cycles at 2.1 second integration with 10 repeated measurements at 250 ppb Ti, this corresponds to 3–4 μg of Ti consumed during a full analysis. Thus, in order to minimize sample consumption during analysis, without compromising the time spend on the actual Ti isotope measurements (as well as V and Cr) in line 2, we measured the Ca interference in line 1 only once at the beginning of each repeated measurement at 33.6 seconds of integration. This limits the amount of Ti consumed per 10 repeats

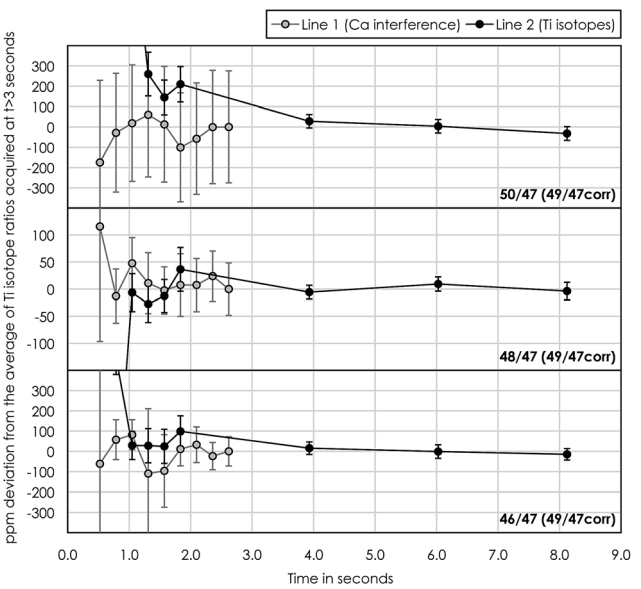

Fig. 9 Test showing the influence of the idle time necessary for the magnet and amplifiers to settle prior to the actual isotope measurements when jumping between peaks in lines 1 (Ca interference) and 2 (Ti isotopes). Internally ^{49}Ti/^{47}Ti normalized mass-fractionation corrected Ti isotope ratios approach constant values after an idle time of ~3 seconds.

Table 6 Ti isotope data summary. The bracketing standard was OL-Ti

Sample	Type of material	μ^{49}Ti	μ^{46}Ti* (49/47)	μ^{48}Ti* (49/47)	μ^{49}Ti* (48/47)	μ^{50}Ti* (49/47)	N [a]
Terrestrial rock standards and samples							
Alfa Aesar Ti	Pure Ti ICP standard from Alfa Aesar	89 ± 16	−9.5 ± 7.5	2.0 ± 5.6	−5.0 ± 10.0	−3.6 ± 8.6	10
BIR-1 (1)	Icelandic basalt, USGS rock standard	−24 ± 12	−11.9 ± 7.6	0.3 ± 4.0	−0.6 ± 8.0	−2.3 ± 5.9	10
BIR-1 (2)	Icelandic basalt, USGS rock standard	−40 ± 19	−3.7 ± 8.4	−1.3 ± 5.3	3.0 ± 10.0	−3.0 ± 9.2	10
BCR-2	Basalt, Columbia River, USGS rock standard	−38 ± 30	−8.3 ± 5.0	2.9 ± 2.6	−6.1 ± 5.2	−3.8 ± 7.7	10
BHVO-2 (1)	Basalt, Hawaiian Volcanic Observatory, USGS rock standard	10 ± 37	4.5 ± 6.6	1.4 ± 2.9	−2.7 ± 5.7	−2.9 ± 7.0	10
BHVO-2 (2)	Basalt, Hawaiian Volcanic Observatory, USGS rock standard	56 ± 11	−2.5 ± 5.3	0.9 ± 3.6	−1.9 ± 7.2	−7.6 ± 5.2	10
Meteoritic samples							
Alfianello	Ordinary chondrite (L6)	180 ± 21	−15.3 ± 8.5	−0.2 ± 5.9	0.0 ± 12.0	−63.8 ± 9.5	8
NWA 6043	CR2 chondrite	1 ± 42	29.9 ± 9.6	−14.0 ± 2.7	27.7 ± 5.4	228.0 ± 10.0	10
31E	CAI from Efremovka ($CV3_{red}$)	270 ± 67	169.5 ± 4.6	34.4 ± 3.5	−68.2 ± 7.0	947.0 ± 12.0	10
Reproducibility test							
A3 (1)	CAI from Allende ($CV3_{ox}$)	479 ± 26	223.0 ± 10.0	8.7 ± 1.7	−17.2 ± 3.4	1459.5 ± 4.3	10
A3 (2)		406 ± 23	232.6 ± 7.9	8.5 ± 2.9	−16.9 ± 5.8	1460.0 ± 10.0	10
A3 (3)		522 ± 32	224.0 ± 13.0	1.6 ± 8.4	−3.0 ± 17.0	1469.8 ± 9.4	10
A3 (4)		397 ± 44	223.0 ± 11.0	12.1 ± 2.7	−23.9 ± 5.4	1470.0 ± 11.0	10
Average and 2sd		***451 ± 120***	***228.2 ± 10.8***	***7.7 ± 8.8***	***−15.3 ± 17.6***	***1464.8 ± 11.7***	

[a] Number of repeated measurements.

to 0.75–1 μg, *i.e.* 4 times less than that by the conventional mode. Hence, the precision of the actual Ti isotope measurements stays the same, because all Ti isotopes are measured in line 2. Although compromising the effectiveness of the Ca interference correction routine, considerably less material is being consumed. This is highly desirable when dealing with very small and unique samples, such as sub-mm-sized CAIs.

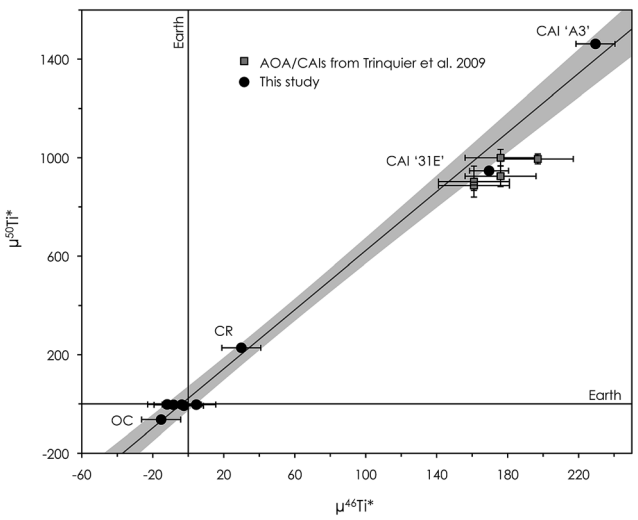

Fig. 10 μ^{50}Ti* *versus* μ^{46}Ti* diagram showing the correlation between inner solar system materials measured in this study (Earth, one ordinary chondrite (Alfianello) and one CR chondrite (NWA 6043)), which is in accordance with the observations of Trinquier *et al.* 2009 and Zhang *et al.* 2011. The correlation extends to include Ca–Al-rich inclusions (CAIs) with divergent anomalies. The CAI, '31E', from the Efremovka CV chondrite has a Ti isotope composition similar to that reported for CAIs and AOAs in Trinquier *et al.* 2009, while the Allende CV CAI, 'A3', shows significantly larger anomalies in both μ^{50}Ti* and μ^{46}Ti*. Error bars are the internal 2se precision or external reproducibility (2sd), whichever is larger.

Reproducibility and accuracy of Ti isotope measurements. Similar to Mg, we used the CV CAI 'A3' to assert the external reproducibility of our chemical and analytical procedures for ~1 μg Ti. Our results show that the stable mass-dependent Ti (μ^{49}Ti) isotope composition can be routinely measured to a precision of ±60 ppm amu^{-1} (2sd, Table 6), which is a factor of 10 better than recent stable Ti isotope data acquired by standard–sample bracketing.[31] Although 6 times larger than the external reproducibility obtained from Ti double-spike techniques,[29] this level of precision is adequate to resolve the μ^{49}Ti variability observed amongst terrestrial magmatic rocks.[4,5] Contrary to double-spike measurements, our approach further enables the combined analysis of both mass-dependent and nucleosynthetic effects on the Ti isotope composition of extraterrestrial rocks. The mass-independent μ^{46}Ti*, μ^{48}Ti*, μ^{49}Ti* and μ^{50}Ti* components can be measured to a precision of 11, 8.8, 18 and 12 ppm, respectively (2sd, Table 6). This is similar to or 2 times better than previous analytical methods on 6–10 times more material.[10] Thus, the 15 000 ppm accuracy limitation on μ^{50}Ti* of our Ti procedures (Fig. 3) fully allows the accurate determination of minor inner solar system isotope signatures, as well as the extreme isotopic signatures in FUN-type CAIs and most hibonite crystals found in carbonaceous chondrites.[7,40,41] Finally, both stable and mass-independent Ti isotope data for terrestrial geostandards (BIR-1, BCR-2 and BHVO-2) are normal within error, demonstrating the accuracy of our methods.

Correlated Ti isotope anomalies in bulk meteorites and CAIs. Significant departures from mass-dependent Ti isotope fractionation have previously been observed for μ^{46}Ti* and μ^{50}Ti* in meteorites and their components.[9–11,42] While inner

solar system materials (bulk chondrites and achondrites) range in μ^{50}Ti* from −200 to +500,[10,42] refractory inclusions (normal CAIs) span a range from ∼+500 to +1600.[10,31,43,44] Our results for one ordinary chondrite (Alfianello, L6) display negative μ^{46}Ti* (−15.3 ± 8.5 [2se]) and μ^{50}Ti* (−63.8 ± 9.5 [2se]) (Table 6) and are in excellent agreement with the results previously reported in Trinquier *et al.* 2009 (ref. 10), Zhang *et al.* 2012 (ref. 42) and Gerber *et al.* 2017.[9] Some variability amongst CR chondrites is reported in the literature, ranging from 140 to 339 ppm in μ^{50}Ti* (9, 10, 30, and 42). This most likely results from heterogeneous sampling of variable amounts of CAI material. Our results for one CR2 chondrite (NWA 6043, μ^{50}Ti* = 228 ± 10 [2se]) are within this range. The two CAIs measured in this study (31E and A3) show resolvable differences in all mass-independent Ti components (Table 6) with 31E displaying a composition (μ^{50}Ti* = 947 ± 12 [2se]) within the range of the data reported in Trinquier *et al.* 2009 (ref. 10) and identical to the median of normal CAIs reported in Davis *et al.* 2017.[31] The other CAI, A3, has larger anomalies in μ^{46}Ti* and μ^{50}Ti* (μ^{50}Ti* = 1464.8 ± 12 [2se], $n = 4$), which is in the upper range of CAI values reported to date. The two CAIs plot on an extension of the correlation line observed amongst inner solar system materials[10] (Fig. 10). Stable Ti isotope data obtained for the two CAIs display positive μ^{49}Ti of a few hundred ppm (Table 6), which is identical to the values reported in Davis *et al.* 2017 (ref. 31) and Simon *et al.* 2017.[44] We note that natural mass-dependent isotope fractionation, which diverges from kinetic processes (*i.e.* follows the exponential fractionation law used for mass bias correction), can potentially generate apparent excesses or deficits in μ^{46}Ti* and μ^{50}Ti*. However, inappropriate mass bias correction associated with mass-dependent fractionation in Ti isotopes can only explain up to ∼3 ppm variability in both μ^{50}Ti* and μ^{46}Ti* per 100 ppm amu^{-1} variation in μ^{49}Ti. Hence, stable isotope fractionation can only explain ∼1% of the variability in μ^{50}Ti* for CAIs, which instead must originate from nucleosynthetic effects.

Conclusions

We have developed a new multi-element ion chromatographic separation protocol, specifically tailored to handle small amounts of isotopically anomalous material, such as Ca–Al-rich inclusions in primitive meteorites, for which impurity contributions must be minimized. We present refined analytical procedures for high-precision Mg and Ti isotope analysis using MC-ICP-MS. The high-precision isotope analysis results of a range of isotopically anomalous chondritic meteorites and refractory inclusions are identical to data previously reported for the same types of materials, demonstrating the accuracy of our methods. Data for terrestrial geostandards are within the error of the OL-Ti standard used for standard–sample bracketing. We show that the protocols allow for the accurate determination of the extreme mass-dependent and mass-independent Mg and Ti isotopic signatures found in both normal CAIs and FUN-type CAIs, as well as some anomalous hibonite crystals in CM chondrites (μ^{26}Mg* up to ±4000 ppm and μ^{50}Ti* up to 15 000 ppm). Finally, our results support the observation of correlated anomalies in μ^{46}Ti* and μ^{50}Ti* for inner solar system materials, which extend to include two CAIs (31E and A3) with highly divergent mass-independent Ti isotope compositions. Such effects cannot be explained by mass-dependent stable isotope fractionation and must invoke variable nucleosynthetic effects in CAIs.

Conflicts of interest

There are no conflicts to declare.

Acknowledgements

We thank Marc-Alban Millet and Christophe Cloquet for providing the OL-Ti standard. Funding for this project was provided through grants from the Danish National Research Foundation (grant number DNRF97) and from the European Research Council (ERC Consolidator grant agreement 616027-STARDUST2ASTEROIDS) to M. B.

Notes and references

1 F.-Z. Teng, *Rev. Mineral. Geochem.*, 2017, **82**, 219–287.
2 J. N. Connelly, M. Bizzarro, A. N. Krot, Å. Nordlund, D. Wielandt and M. A. Ivanova, *Science*, 2012, **338**, 651–655.
3 K. K. Larsen, M. Schiller and M. Bizzarro, *Geochim. Cosmochim. Acta*, 2016, **176**, 295–315.
4 M.-A. Millet, N. Dauphas, N. D. Greber, K. W. Burton, C. W. Dale, B. Debret, C. G. Macpherson, G. M. Nowell and H. M. Williams, *Earth Planet. Sci. Lett.*, 2016, **449**, 197–205.
5 N. D. Greber, N. Dauphas, A. Bekker, M. P. Ptáček, I. N. Bindeman and A. Hofmann, *Science*, 2017, **357**, 1271–1274.
6 M. Schiller, J. A. Dallas, J. Creech, M. Bizzarro and J. A. Baker, *Geochemical Perspectives Letters*, 2017, 22–31.
7 M.-C. Liu, K. D. McKeegan, J. N. Goswami, K. K. Marhas, S. Sahijpal, T. R. Ireland and A. M. Davis, *Geochim. Cosmochim. Acta*, 2009, **73**, 5051–5079.
8 E. M. M. E. Van Kooten, D. Wielandt, M. Schiller, K. Nagashima, A. Thomen, K. K. Larsen, M. B. Olsen, Å. Nordlund, A. N. Krot and M. Bizzarro, *Proc. Natl. Acad. Sci. U. S. A.*, 2016, **113**, 2011–2016.
9 S. Gerber, C. Burkhardt, G. Budde, K. Metzler and T. Kleine, *Astrophys. J.*, 2017, **841**, L17.
10 A. Trinquier, T. Elliott, D. Ulfbeck, C. Coath, A. N. Krot and M. Bizzarro, *Science*, 2009, **324**, 374–376.
11 F. R. Niederer, D. A. Papanastassiou and G. J. Wasserburg, *Astrophys. J.*, 1980, **240**, L73–L77.
12 V. Mavromatis, A. Immenhauser, D. Buhl, B. Purgstaller, A. Baldermann and M. Dietzel, *Geochim. Cosmochim. Acta*, 2017, **207**, 139–153.
13 A. M. Davis and F. M. Richter, in *Treatise on Geochemistry*, Elsevier Ltd., 2nd edn, 2014, vol. 1, pp. 335–360.
14 J. Zhang, S. Huang, A. M. Davis, N. Dauphas, A. Hashimoto and S. B. Jacobsen, *Geochim. Cosmochim. Acta*, 2014, 1–47.

15 K. K. Larsen, A. Trinquier, C. Paton, M. Schiller, D. Wielandt, M. A. Ivanova, J. N. Connelly, Å. Nordlund, A. N. Krot and M. Bizzarro, *Astrophys. J., Lett.*, 2011, **735**, L37.
16 M. Schiller, J. N. Connelly, A. C. Glad, T. Mikouchi and M. Bizzarro, *Earth Planet. Sci. Lett.*, 2015, **420**, 45–54.
17 J. Bollard, J. N. Connelly, M. J. Whitehouse, E. A. Pringle, L. Bonal, J. K. Jørgensen, Å. Nordlund, F. Moynier and M. Bizzarro, *Sci. Adv.*, 2017, **3**, e1700407.
18 J. Zhang, N. Dauphas, A. M. Davis and A. Pourmand, *J. Anal. At. Spectrom.*, 2011, **26**, 2197.
19 D. Wielandt and M. Bizzarro, *J. Anal. At. Spectrom.*, 2011, **26**, 366.
20 N. S. Saji, D. Wielandt, C. Paton and M. Bizzarro, *J. Anal. At. Spectrom.*, 2016, 1–20.
21 F. Nelson, T. Murase and K. A. Kraus, *J. Chromatogr.*, 1964, **13**, 503–535.
22 K. K. Larsen, D. Wielandt, M. Schiller and M. Bizzarro, *J. Chromatogr. A*, 2016, **1443**, 162–174.
23 M. Bizzarro, C. Paton, K. K. Larsen, M. Schiller, A. Trinquier and D. Ulfbeck, *J. Anal. At. Spectrom.*, 2011, **26**, 565.
24 F. W. E. Strelow, A. H. Victor, C. R. Van Zyl and C. Eloff, *Anal. Chem.*, 1971, **43**, 870–876.
25 A. Pourmand and N. Dauphas, *Talanta*, 2010, **81**, 741–753.
26 A. Makishima, X.-K. Zhu, N. S. Belshaw and R. K. O'Nions, *J. Anal. At. Spectrom.*, 2002, **17**, 1290–1294.
27 M. B. Olsen, M. Schiller, A. N. Krot and M. Bizzarro, *Astrophys. J.*, 2013, **776**, L1.
28 C. Paton, J. Hellstrom, B. Paul, J. Woodhead and J. Hergt, *J. Anal. At. Spectrom.*, 2011, **26**, 2508.
29 M.-A. Millet and N. Dauphas, *J. Anal. At. Spectrom.*, 2014, **29**, 1444–1458.
30 I. Leya, M. Schönbächler, U. Wiechert, U. Krähenbühl and A. N. Halliday, *Int. J. Mass Spectrom.*, 2007, **262**, 247–255.
31 A. M. Davis, J. Zhang, N. D. Greber, J. Hu, F. L. H. Tissot and N. Dauphas, *Geochim. Cosmochim. Acta*, 2017, 275–295.
32 A. Galy, N. S. Belshaw, L. Halicz and R. K. O'Nions, *Int. J. Mass Spectrom.*, 2001, **208**, 89–98.
33 T. Lee, D. A. Papanastassiou and G. J. Wasserburg, *Astrophys. J., Lett.*, 1977, **211**, L107–L110.
34 M. Bizzarro, J. A. Baker and H. Haack, *Nature*, 2004, **431**, 275–278.
35 D. Wielandt, K. Nagashima, A. N. Krot, G. R. Huss, M. A. Ivanova and M. Bizzarro, *Astrophys. J.*, 2012, **748**, L25.
36 J. Holst, M. B. Olsen, C. Paton, K. Nagashima, M. Schiller, D. Wielandt, K. K. Larsen, J. N. Connelly, J. K. Jørgensen, A. N. Krot, Å. Nordlund and M. Bizzarro, *Proc. Natl. Acad. Sci. U. S. A.*, 2013, **110**, 8819–8823.
37 M. Schiller, C. Paton and M. Bizzarro, *Geochim. Cosmochim. Acta*, 2015, **149**, 88–102.
38 M. Schiller, J. A. Baker and M. Bizzarro, *Geochim. Cosmochim. Acta*, 2010, **74**, 4844–4864.
39 R. C. Hin, C. D. Coath, P. J. Carter, F. Nimmo, Y.-J. Lai, P. A. E. P. von Strandmann, M. Willbold, Z. M. Leinhardt, M. J. Walter and T. Elliott, *Nature*, 2017, **549**, 511–515.
40 T. R. Ireland, *Geochim. Cosmochim. Acta*, 1990, **54**, 3219–3237.
41 L. Kööp, D. Nakashima, P. R. Heck, N. T. Kita, T. J. Tenner, A. N. Krot, K. Nagashima, C. Park and A. M. Davis, *Geochim. Cosmochim. Acta*, 2017, 1–44.
42 J. Zhang, N. Dauphas, A. M. Daivs, I. Leya and A. Fedkin, *Nat. Geosci.*, 2012, **5**, 251–255.
43 C. D. Williams, P. E. Janney, R. R. Hines and M. Wadhwa, *Chem. Geol.*, 2016, **436**, 1–10.
44 J. I. Simon, M. K. Jordan, M. J. Tappa, E. A. Schauble, I. E. Kohl and E. D. Young, *Earth Planet. Sci. Lett.*, 2017, **472**, 277–288.